Jestr

Journal of Engineering Science and Technology Review 16 (3) (2023) 199 - 206

Research Article

JOURNAL OF
Engineering Science and Technology Review

www.jestr.org

Numerical Simulation of Flow-induced Vibration of a Rotating Detonation Engine

Bo Xiang and Yuhui Wang*

College of Mechanical and Electrical Engineering, Beijing University of Chemical Technology, Beijing 100029, China

Received 19 March 2023; Accepted 3 July 2023

Abstract

Rotating detonation engines can be used as rocket engines or air-breathing engines. Extensive research has focused on the flow field and combustion inside the engine, but studies on the flow-induced vibration of the structure are limited. In this study, the flow-induced structural vibration of a rotating detonation engine under the shock wave pressure load was investigated by presenting a unidirectional fluid-solid coupling numerical model. Three cases were explored in the structural analysis, considering the effect of wall thickness on vibration. Numerical simulations of the flow field in the engine used a hydrogen-air model. The flow pressure distributed on the coupled interface between the flow and structure, in which the dynamic load acted, was extracted, and then modal and transient structure simulations were carried out. Results show clear logical connections between the vibration of the combustor component and the excitation of the flow pressure. The propagation frequency of the shock wave is the same as the vibration frequency. The fundamental frequency increases and the vibration intensity decreases as the wall thickness of the component increases, thereby indicating that increasing the wall thickness can reduce the structural vibration.

Keywords: rotating detonation engine, fluid-structure interaction, flow-induced vibration, simulation

1. Introduction

Rotating detonation engines (RDEs) using detonation combustion mode are at the forefront of pressure gain combustion research [1]; they have shown great potential in propulsion systems [2]. Detonation is pressurized combustion, which can theoretically increase the thermodynamic cycle efficiency by more than 20% compared with the deflagration mode used in conventional engines [3]. Unreacted fuel inside the combustor is directly pressurized by the rotating detonation wave (RDW), which has the characteristics of a high-pressure rise with cyclic propagation [4], requiring only one ignition [5]. The pressurization equipment, such as a compressor, is eliminated to obtain a more compact RDE. A Japanese team [6] has successfully created an RDE system for sounding rockets and operated it in a space environment for the first time.

Fig. 1 highlights a typical RDE flow field, where the fuel and oxidizer are injected at the inlet of the annular chamber. The RDW can propagate continuously along the circumference when the fuel is ignited. A contact surface is produced after the collision of the RDW and the interface between the reactant and the product. The oblique shock wave is a refracted wave given that the RDW collides with the interface.

In this study, the analysis is separated into the computational fluid dynamics (CFD) simulation of the flow field and transient structural, modal analysis of the combustor wall to examine the flow-induced vibration of an RDE. Initially, a 3D annular RDE model was established to obtain the flow pressure for hydrogen–air premixed combustion. Then, the pressure along the outer wall surface of the annular chamber was extracted as the excitation load into the finite element method (FEM) model, which was built to analyze the structural dynamic response of the combustor. In addition, the effect of different wall thicknesses on the vibration was analyzed. The natural vibration characteristics under the corresponding constraints were also investigated, and their relationship with the RDW propagation frequency was explored to avoid structural damage caused by resonance.

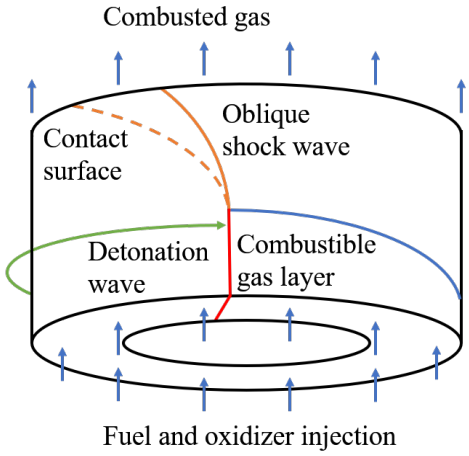

Fig. 1. Schematic of the RDE flow field

2. Literature review

Extensive research has focused on the rotating detonation flow field and combustion, including factors such as propellant mass flow rate, combustion chamber configuration, reactant injection scheme, combustion chamber outlet backpressure, the pressure loss of oxidant

*E-mail address: xiangbo9812@163.com
ISSN: 1791-2377
doi:10.25103/jestr.163.24

and fuel, and detonation wave initiation that affect the propagation and stability of RDW, but the vibration and deformation of the combustor have not been studied in detail. At present, research is mainly conducted on the propagation mechanism of detonation waves, RDE propulsion performance [7], combustion chamber thermal protection [8], and RDE thermal efficiency [9] through experimental measurements, numerical simulations, and theoretical analysis.

Bykovskii et al. [10] demonstrated and analyzed the feasibility of vibration monitoring in RDE by measuring the noise and vibration levels of a rotating detonation combustor (RDC). Furthermore, Zhong et al. [11] investigated the relationship between vibration and RDW propagation modes. They proposed that vibration sensors could provide a new potential method for mode monitoring of transient RDW in long-term operation. Sawad et al. [12] concluded that the tangential friction between the RDW and the chamber wall resulted in a torque around the z-axis except for thrust. They also elucidated the connection between the direction and intensity of the torque with RDW propagation modes.

Detonation led to the formation of products with high energy density, whose intense dilatant flow was the fundamental cause of the RDE thrust. The pressure generated by shock waves with propagation speeds of 1-3 km/s [13] acted directly on the combustor walls, causing structural vibrations. Wang et al. [14] pointed out that the RDE internal flow is an unsteady flow, which must be accompanied by a corresponding forced vibration. The propagation of RDW and oblique shock wave will induce the RDE to exhibit conical pendulum motion. Shock waves generated extremely localized loads that resulted in path-dependent aeroelastic behavior evolving over the life of the structure, and this interaction is a crucial issue in the design of flight-weight structures [15]. Aeroelastic response analysis of the RDE was beneficial for the safe and reliable operation of propulsion systems. Structural vibration under the action of flow pressure is a typical fluid–solid interaction (FSI) problem. Malla et al. [16] applied the flow pressure loads generated by CFD simulation into structural and modal analysis to disclose the structural response of the nozzle during supersonic operation.

Experimental studies of RDE vibration and forces are mentioned above. Stopka et al. [17] developed a FEM model to analyze the fatigue response and evaluate the expected fatigue life of an RDC liner. Moreover, they modeled the flow pressure loading conditions as cycle-to-cycle canonical waveforms. In contrast, this study calculates the flow field of the detonation wave, which can more accurately reflect the pressure conditions acting on the structure. And the geometric model in [17] is a thirteenth part setting as an axisymmetric structure for analysis, while the geometric model matching the load in this paper is a complete circular structure.

3. Methodology

3.1 Governing equations and numerical methods for fluid

Only gas dynamic properties were considered [11], ignoring viscosity, heat conduction, and mass diffusion. The governing equations of mass conservation, momentum conservation, energy conservation, species transport, and ideal gas equation of state are expressed as follows [12-13]:

$$\frac{\partial \rho}{\partial t}+\nabla\cdot(\rho V)=0 \tag{1}$$

$$\frac{\partial}{t}(\rho V)+\nabla\cdot(\rho VV)+\nabla p=0 \tag{2}$$

$$\frac{\partial}{\partial t}[\rho(e+\frac{v^2}{2})]+\nabla\cdot[\rho V(e+\frac{v^2}{2}))+\nabla\cdot(pV)=S_h \tag{3}$$

$$\frac{\partial}{\partial t}(\rho Y_i)+\nabla\cdot(\rho VY_i)=\dot{\omega}_i \quad (i=1,\cdots,N-1) \tag{4}$$

$$p=\rho RT \tag{5}$$

where t is time, V is the velocity vector, v is the modulus of V, ρ is density, p is pressure, e is the internal energy, S_h is the energy source term, Y_i is the mass fraction of component i, N is the total fraction, $\dot{\omega}_i$ is the net rate of production of species i by chemical reaction, R is the gas constant, and T is temperature.

The laminar finite-rate model with a one-step reaction of hydrogen and air is used to determine the chemical reactions, where $H_2+O_2+3.76N_2=2H_2O+3.76N_2$, and the backward reaction was not considered. Arrhenius formula, which was exactly designed for laminar flames, was used to calculate the source term of the chemical reactions, ignoring the effect of turbulent fluctuations on reactions [14]. The forward rate constant $k_{f,r}$ for the chemical reaction r can be calculated by the Arrhenius expression, as follows:

$$k_{f,r}=A_rT^{\beta r}\exp(-E/RT) \tag{6}$$

where Ar is the pre-exponential factor, βr is the temperature exponent (dimensionless), and Er is the activation energy for the reaction (J/kmol).

A time step of 0.01 μs was used, and the courant number was limited to ensure that the computations can converge. The boundary conditions included a mass flow inlet [15] and a pressure outlet, and all walls were slip boundaries and adiabatic [16-17]. The activation energy of the chemical reaction was set to Er=5.5×107 J/mol when the flow field was stabilized. A high-temperature and high-pressure ignition region was patched at 2000 K and 2 MPa, respectively, when the RDE has been filled with premixed gas.

An unsteady density-based solver was used given the high-speed compressible flow in the RDE. The convective flux was solved using the advection upstream splitting method (AUSM) [18], which can accurately capture contact surfaces and shock waves without oscillations. The transient formulation used the second-order implicit method, which combined the central difference scheme and the second-order upwind scheme.

3.2 Governing equations and numerical methods for vibration

Assuming that the structure is a linear elastic body in a small deformation, the governing equation for vibration is as follows [19]:

$$M\ddot{u}+C\dot{u}+Ku=F(t) \tag{7}$$

where M is the mass matrix, C is the damping matrix, K is the stiffness matrix, and $F(t)$ is the applied force; $\ddot{u}$, $\dot{u}$, and u represent the nodal acceleration, velocity, and displacement vectors, respectively.

In the modal analysis, dynamic loading is not required and the nonlinear properties are neglected. Furthermore, structural damping slightly affects the natural frequency, and this effect can be ignored. Thus, Eq. (7) is simplified as follows:

$$M\ddot{u} + Ku = 0 \tag{8}$$

The free vibration equation for an elastic body can be decomposed into a series of superpositions of simple harmonic vibrations, as follows:

$$(K - \omega^2 M)u = 0 \tag{9}$$

where ω^2 and u are the generalized eigenvalues and eigenvectors, respectively, satisfying the above equation.

The inlet wall of the RDE was considered fixed support, which was used to constrain the six directions of freedom. The outer wall was subjected to a constant standard atmospheric pressure. The inner wall was the FSI coupling interface with flow pressure loads of 600-780 μs obtained from CFD simulation. The gravity was set in the positive direction along the x-axis. Stainless steel was selected as the material. The transient structure calculation applied the iterative preconditioned conjugate gradient (PCG) solver [10], and the time step was set to 0.125 μs.

In accordance with the RDE model, the modal analysis was carried out by removing the applied force to solve the structural inherent characteristics, including the structural natural frequency and mode shape that provide a preliminary estimate of the possible dynamic response of the structure under excitation.

A simplified RDE model is shown in Fig. 2. The radius of the center body is 5.0 mm, the annular width is 10.0 mm, the axial length is 15.0 mm, and the solid wall thickness is w, (w=5.0, 7.0, 9.0 mm). The coordinate system in Fig. 2 was used for structural analysis, and the origin was located at the center of the cylinder inlet.

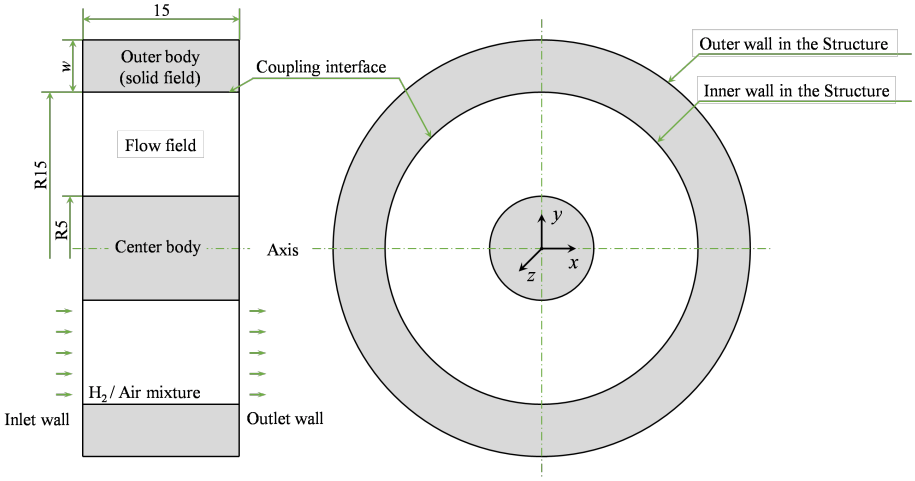

Fig. 2. Schematic of RDE geometry

3.3 Grid independence verification

Three cell sizes at 0.40, 0.25, and 0.20 mm were used to verify the grid independence for the flow study, and the results are shown in Table 1. The difference in the average RDW temperature among the three models is less than 2.00%. Moreover, the errors of RDW velocities for the three cell sizes are less than 0.50%. Fig. 3 presents the pressure contours of the cross-section (z=4.0 mm) at 20 μs for different cell sizes. The results show that the flow fields are similar to each other. Thus, the grid with a cell size of 0.20 mm was used for the CFD simulations.

Three different cell sizes (0.50, 0.25, and 0.20 mm) using SOLID186 were tested to verify the mesh independence in the structure analysis. The equivalent stress (calculated by Eq. 10) and deformation traces under the flow pressure load at a monitoring point (15.0, 0, and 4.0 mm) are shown in Fig. 4, and a local magnification of the peak is presented on the right.

$$\sigma_e = \sqrt{\frac{1}{2}[(\sigma_x - \sigma_y)^2 + (\sigma_y - \sigma_z)^2 + (\sigma_z - \sigma_x)^2 + 6(\sigma_{xy}^2 + \sigma_{yz}^2 + \sigma_{xz}^2)]} \tag{10}$$

Where σ_e is equivalent stress; σ_x , σ_x , and σ_x are direct stresses; σ_x , σ_x , and σ_x are shear stresses. The errors of the equivalent stress are within 3.30%, and those of the deformation are within 2.60%. The cell size of 0.25 mm was adopted for the FEM model, considering the mesh matching condition of the coupling interface.

Table 1. Parameters of RDW for different cell sizes

Cell size, mm	Cell amount	RDW velocity, m/s	RDW temperature, K
0.20	926250	2357	3460
0.25	483120	2350	3421
0.40	117800	2344	3393

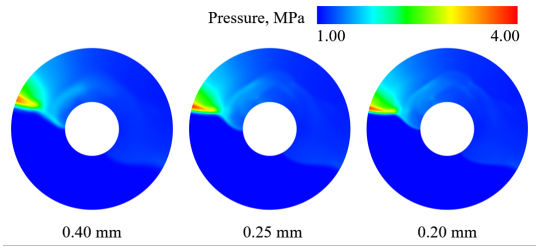

Fig. 3. Pressure contours for different cell sizes

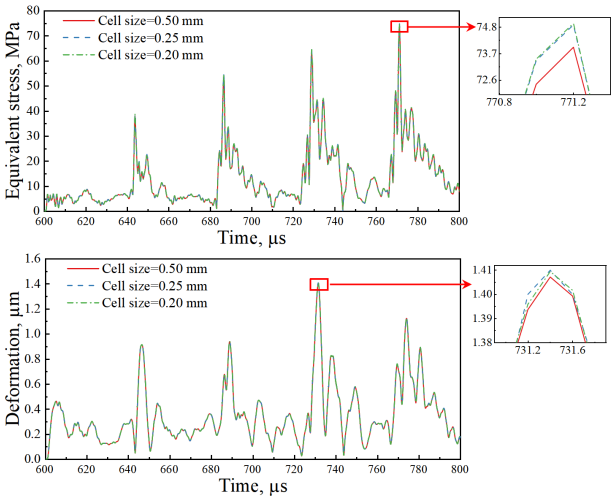

Fig. 4. Traces of equivalent stress and deformation for different cell sizes

4. Results analysis and discussion

This section discusses the flow field characteristics of a 3D hydrogen/air detonation inside the RDE, in particular the flow field and pressure distribution on the coupling interface. This work focuses on the structural analysis of the RDE. The structure modes without load were studied initially. Then, the RDW pressure field was coupled to the FEM model. The RDE is a forced vibration system, where the RDW was considered an excitation load. Moreover, the effect of the wall thickness on the vibration was investigated by varying w (w=5.0, 7.0, 9.0 mm).

4.1 RDE flow field

A single RDW was produced after ignition, and the RDW propagates counterclockwise. Fig. 5 shows the pressure and temperature traces of the RDW at a monitoring point (15.0, 0, and 4.0 mm) with more than 14 complete cycles. The propagation frequency and velocity of the RDW were calculated by Eqs. (11) and (12), as follows:

$$f_{RDW} = \frac{1}{T_{RDW}} \tag{11}$$

$$v_{RDW} = Lf_{RDW} \tag{12}$$

where f_{RDW} is the RDW frequency, v_{RDW} is the RDW velocity, T_{RDW} is the cycle time, and L is the circumference of the outer wall surface, 30π mm.

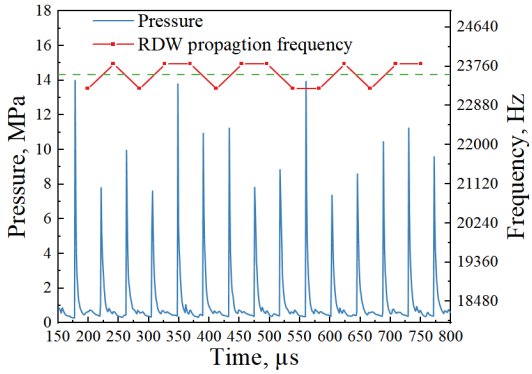

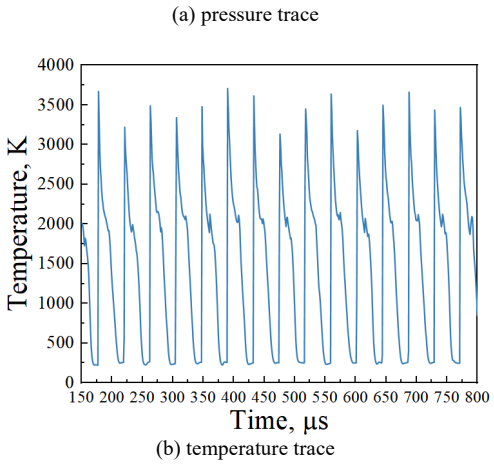

Fig. 5. Pressure and temperature traces at a monitoring point

In Fig. 5 (a), the RDW frequency oscillates around the average propagation frequency of 23572 Hz. The corresponding average wave velocity of 2221.6 m/s is higher than the theoretical Chapman-Jouget (C-J) detonation wave velocity of 2069.9 m/s (with an error of 7.00%), which is also found in the previous study. The pressure peaks fluctuate owing to transverse waves moving along the detonation, as shown in Fig. 5 (a).

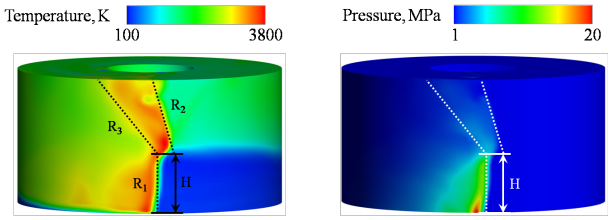

Fig. 6. Temperature and pressure contours for the flow

Fig. 6 displays the contours of pressure and temperature for the flow field up to 715 μs, where the dashed line illustrates the RDW, oblique shock wave, and contact surface. A single RDW, denoted by R_1, is observable, with a height h of approximately 6.5 mm. The hydrogen-air mixture forms a triangular region in front of the RDW because the RDW of high pressure blocks the flow. The oblique shock wave of R_2 is a refracted wave of the RDW colliding with the interface between the reactant and product. After the detonation, the burnt products expand azimuthally and axially, and then ultimately flow out from the outlet surface. The flow has a strong cyclic and circumferential aspect due to the detonation wave propagation [20]. A contact surface of R_3 exists between the fresh detonation products and older products.

The RDW has a higher pressure near the outer side of the flow channel, where it is compressed. The flow pressure given the dynamic load on the coupling interface is directly related to the further structural dynamic response. Instantaneous unwrapped 2D slices with pressure contours for a cycle are shown in Fig. 7. Extreme pressure occurs in the RDW front, whereas a high-pressure triangle region is found behind the RDW. This finding is caused by the Taylor expansion waves and reflected expansion waves from the interface between the reactant and the product. Meanwhile, the pressure peaks and the RDW heights fluctuate within one cycle due to the interference of the transverse waves.

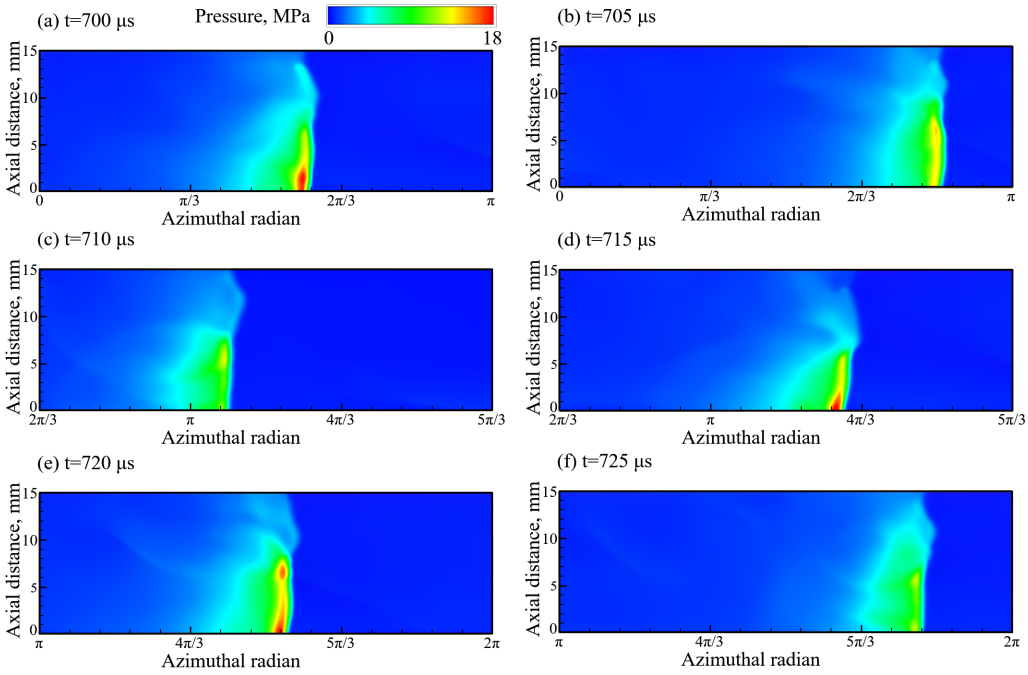

Fig. 7. Pressure contours at the fluid-solid coupling interface of the inner wall

4.2 Structural modes of the RDE

The periodic pressure load acting on the coupling interface at 600-780 μs was obtained from the flow field. This load propagated at an average frequency of 23669 Hz, which is much lower than the initial structural natural frequencies of 30424, 34549, and 37746 Hz for different wall thicknesses (w=5.0,7.0,9.0m, respectively). The ratios of the excitation frequency to the three natural frequencies were 0.78, 0.68, and 0.63, indicating that no resonance is present in this forced vibration system. Moreover, the initial frequency increases with the increasing wall thickness, and the stiffness remarkably increases, resulting in a more resistant structure to excitation.

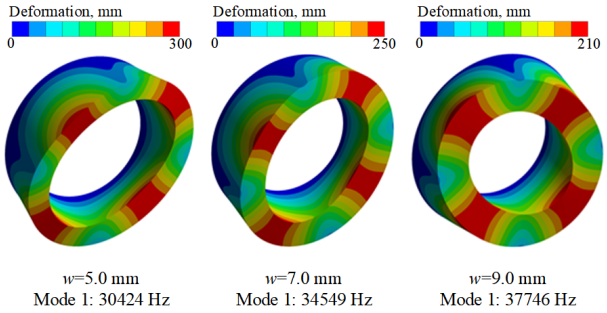

Fig. 8. Initial mode shapes of the RDC component

Fig. 8 shows the first mode of the RDC component model under free vibration. The highest deflection occurs on the outlet surface. Scaling the characteristic vectors proportionally does not affect the satisfaction of the characteristic equation because the vibration equation in Eq. (9) is a homogeneous equation. Therefore, the obtained characteristic vectors do not represent the actual deformation vectors but only depict the deformation shapes. In actual vibration, multiple modes can coexist, resulting in more complex mode shapes.

4.3 Structural dynamic response

The transient load of this forced vibration system at 600–780 μs, which is more than four RDW cycles, was applied to the coupling interface. In this section, the resulting coordinate system is altered to a cylindrical coordinate system, with the origin and x-axis position unchanged, as shown in Fig. 9. The flow pressure load trace at a monitoring point of P_1 (15.0 mm, π/6, 4.0 mm) is shown in Fig. 10 (a). In Fig. 10 (b), the stress traces of Norm X, Y, and Z at the same point P_1 denote the radial, tangential, and axial stresses, respectively. The RDW with a high pressure acting on the structure results in an upsurge in stress. The normal stresses in the tangential and axial directions are remarkably higher than the aforementioned pressure and difficult to stabilize at zero after the wavefront.

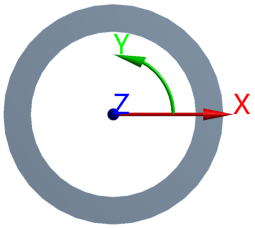

Fig. 9. Cylindrical coordinate system

For the wall thickness of w=5 mm, the traces of the deformation and acceleration at the monitoring point of P_1 are illustrated in Figs. 11 (a) and (c). Under the influence of shock waves and the interaction between masses, the curves oscillate around zero and reach peaks when the RDW passes the monitoring point. In addition, the curves reveal an unequivocal periodicity, indicating that the RDE vibrates periodically about the original position under the RDW excitation. The pressure trace of the flow load in Fig. 10 (a) and the corresponding radial deformation and radial acceleration are shown in Figs. 11 (b) and (d). The average propagation frequency of the flow pressure load is f_{RDW}=23669 Hz, the frequency deformation peak is f_d=23529 Hz, and their ratio is f_d/f_{RDW}=0.99. When a structure undergoes forced vibration, the frequency of the forced

response is equal to that of the excitation load. This type of correlation is caused by the dominant state of the RDW in the vibration sources. The pressure peaks occur a few microseconds earlier than the peaks of radial deformation in Fig. 11 (b) because the deformation production requires considerable time after the interaction between the RDW and structure given that acceleration is the second derivative of deformation.

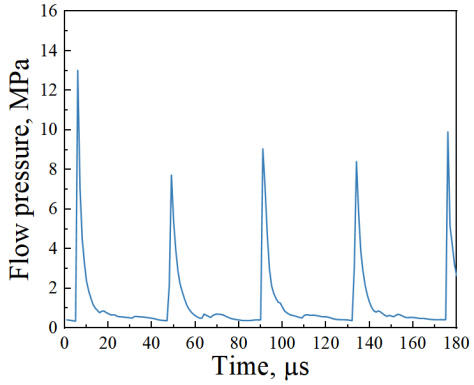

(a) flow pressure trace

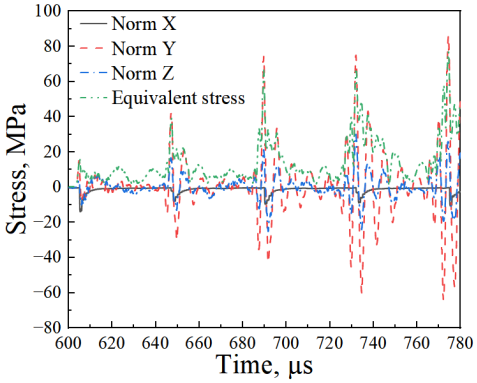

(b) stress trace

Fig. 10. Flow pressure and structure stress at the monitoring point P1

The start–end time in structural simulation follows the time range of the extracted pressure load, which is continuous around the moment zero. However, the state before the moment zero and the initial position at the moment zero cannot be accurately ascertained; thus, the curves at the beginning are not at their realistic states.

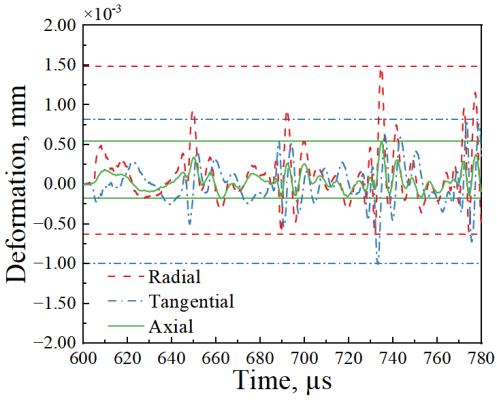

(a) deformation traces

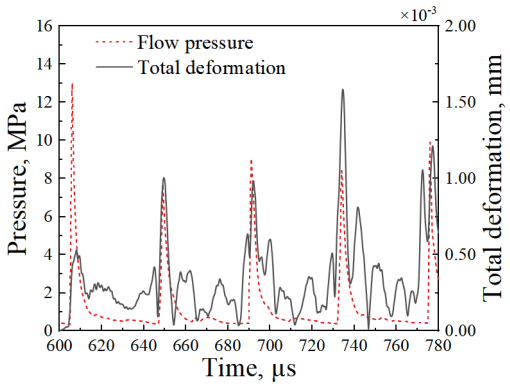

(b) flow pressure and radial deformation traces

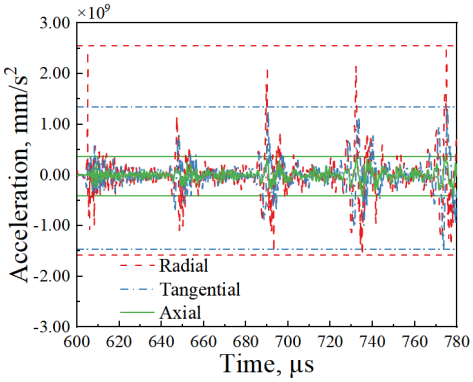

(c) acceleration traces

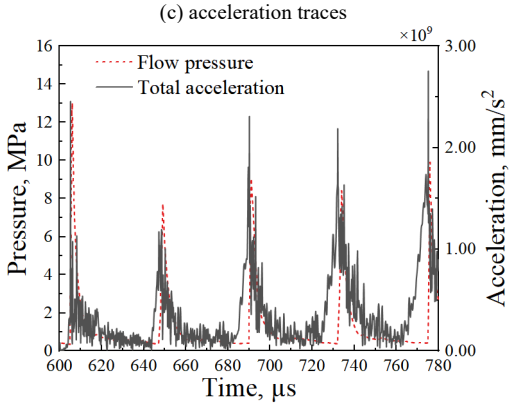

(d) flow pressure and radial acceleration traces

Fig. 11. Deformation, flow pressure, and acceleration at the monitoring point P_1

4.4 Effects of wall thickness

The total velocity traces at the monitoring point of P_2 (n, π/6, 7.5 mm) (n=17.5, 18.5, 19.5 mm) that determine the effect of wall thickness on the vibration are shown in Fig. 12 (a), exhibiting the same periodicity as the RDW in this forced vibration system. The corresponding scatter plot is shown in Fig. 12 (b), where the vibration peaks of the different cases are marked and connected with a gray line. The peaks of velocity caused by the shock wave decrease as the wall thickness increases. Increasing wall thickness increases the stiffness, correspondingly reducing the amplitude of the response vibration. Therefore, increasing the wall thickness is beneficial for the RDE to reduce vibration. The deviation between the propagating frequency of the detonation wave and the natural frequency of the combustor is the main factor for the nonlinear variation trend [21], as shown in Fig. 13.

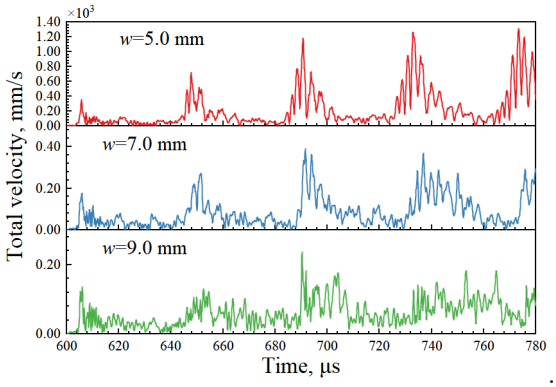

(a) traces of total velocity

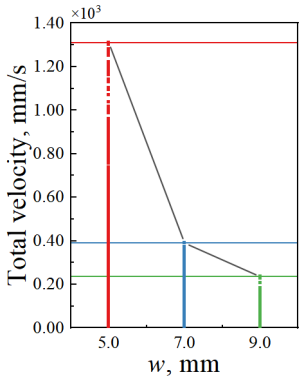

(b) scatter plot of total velocity

Fig. 12. Total deformation at monitoring point P_2 for different w

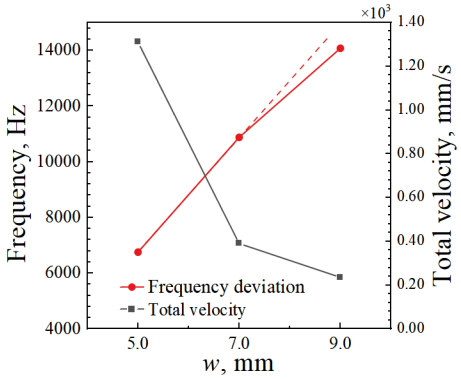

Fig. 13. Total velocity and frequency deviation vary with changes in wall thickness

The maximum equivalent stress traces are plotted in Fig. 14, validating whether the maximum stress of the FEM exceeds the strength limit of the material. The equivalent stress of the case w=5.0 mm is significantly higher than those of the two other cases. The maximum equivalent stresses for the wall thickness of 5.0, 7.0, and 9.0 mm are 129.9, 77.8, and 77.0 MPa, respectively. None of them exceeds the yield strength of 207 MPa for stainless steel.

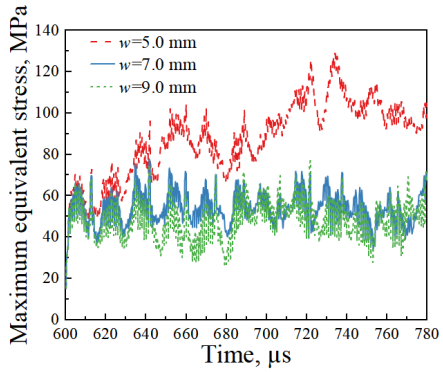

Fig. 14. Traces of maximum equivalent stress

5. Conclusion

In this study, the unidirectional FSI simulation method was applied to investigate the flow-induced vibration characteristics of the RDE, which has not been studied in detail previously. This approach is a key initial step to evaluate the structural dynamic response of RDE components. Numerical simulations of the 3D flow field inside the RDE using hydrogen and air, a modal analysis, and transient structure analysis were carried out successively. The effect of the wall thickness on vibration was also studied.

This forced vibration system does not exhibit resonance. In addition, increasing the wall thickness of the RDE results in a more stable structure because the increased natural frequency of the structure caused a larger deviation between the excitation frequency and the natural frequency increased. In actual vibration, multiple modes coexist, resulting in more complex mode shapes.

On the fluid–solid coupling interface inside the combustor, the RDW, oblique shock wave, and contact surface occur. The high-pressure triangular region occurs behind the detonation wave, and the peak pressure is observed on the RDW. The traces of structural deformation and acceleration under the RDW flow pressure load are periodic, with the frequency of the forced response equal to that of the excitation load. This type of correlation is caused by the dominant state of the RDW in the vibration sources. Increasing the wall thickness of the RDE reduces the amplitudes of deformation and acceleration caused by the RDW, resulting in a more stable structure.

The simulation method of FSI is applied for the first time to study the vibration response of RDC, but the numerical and geometric models are simplified to a certain extent. Nevertheless, this study is objectively deficient and has certain limitations. The governing equation of the flow field ignores the effect of viscosity. The shear force and axial torque caused by friction between the fluid and the chamber wall are not considered. Thus, detailed experiments are required to study the vibration of RDE.

Acknowledgments

This study is supported by the Special Fund for Basic Research Operations of Central Universities (No. buctrc201913).

References

1. Anand, V., Gutmark, E., "Rotating detonation combustors and their similarities to rocket instabilities". *Progress in Energy and Combustion Science*, 73, 2019, pp.182-234.
2. Zhou, R., Wu, D., Wang, J., "Progress of continuously rotating detonation engines". *Journal of Aerospace Power,* 29(1), 2016, pp.15-29.
3. Sousa, J., Paniagua, G., Morata, E. C., "Thermodynamic analysis of a gas turbine engine with a rotating detonation combustor". *Applied Energy*, 195, 2017, pp.247-256.
4. Wolański, P., "Detonative propulsion". *Proceedings of the Combustion Institute*, 34(1), 2013, pp.125-158.
5. Zheng, Y., Wang, C., Wang Y., Le, J., "Numerical research of rotating detonation initiation processes with different injection patterns". *Journal of Propulsion Technolog*. (2), 2019, pp.407-415.
6. Goto, K., Matsuoka, K., Matsuyama, K., Kawasaki, A., Watanabe, H., Itouyama, N., Ishihara, K., Buyakofu, V., Noda, T., Kasahara, J., Matsuo, A., "Space flight demonstration of rotating detonation engine using sounding rocket S-520-31". *Journal of Spacecraft and Rockets*, 60(1), 2023, pp.273-285.
7. Smith, R. D., Stanley, S. B., "Experimental investigation of rotating detonation rocket engines for space propulsion". *Journal of Propulsion and Power*, 37(3), 2021, pp.463-473.
8. Frolov, S. M., Shamshin, I. O., Aksenov, V. S., Gusev, P. A., Zelensky, V. A., Evstratov, E. V., Alymov, M. I., "Rocket engine with continuously rotating liquid-film detonation". *Combustion Science and Technology,* 192(1), 2018, pp. 144-165.
9. Stechmann, D. P., Heister, S. D., Harroun, A. J., "Rotating detonation engine performance model for rocket applications". *Journal of Spacecraft and Rockets*, 56(3), 2019, pp.887-898.
10. Bykovskii, F. A., Vedernikov, E. F., Polozov, S. V., "Noise and vibrations in a combustor with continuous spin detonation combustion of the fuel". *Combustion, Explosion and Shock Waves*, 42, 2006, pp.582-593.
11. Zhong, Y., Wu, Y., Jin, D., "Rotating detonation mode recognition using non-intrusive vibration sensing". *Energy,* 199, 2020, pp.117466.
12. Sawada, S., Kawasaki, A., Matsuoka, K., Kasahara, J., Matsuo, A., Funaki, I., "Experimental measurement of torque and force on a rotating detonation engine with six-axis force sensor". In: *AIAA Scitech 2021 Forum*, Virtual Event: American Institute of Aeronautics and Astronautics, 2021, pp.0295.
13. Hargus, W. A., Schumaker, S. A., Paulson, E. J., "Air force research laboratory rotating detonation rocket engine development". In: *2018 Joint Propulsion Conference*, Cincinnati, USA: American Institute of Aeronautics and Astronautics, 2018, pp.4876.
14. Wang, Y., Le, J., "Experimental study of sharp noise caused by rotating detonation waves". *Noise Control Engineering Journal*, 70(6), 2022, pp.527-539.
15. Brouwer, K. R., Perez, R. A., Beberniss, T. J., Spottswood, S. M., Ehrhardt, D. A., "Evaluation of reduced-order aeroelastic simulations for shock-dominated flows". *Journal of Fluids and Structures*, 108, 2022, pp.103429.
16. Malla, B., Holder, J., Anand, V., Gutmark, E., "Structural excitation of SERNs during supersonic operation: A source of screech amplitude modulation". *Journal of Fluids and Structures*, 107, 2021, pp.103390.
17. Stopka, K., Smallwood, J., Chokshi, A., Heister, S. D., Sangid, M., "Structural and fatigue analysis of a rotating detonation rocket engine". In *AIAA Scitech 2023 Forum,* National Harbor, USA: American Institute of Aeronautics and Astronautics, 2023, pp.1869.
18. Yi, T. H., Lou, J., Turangan, C., Choi, J. Y., Wolanski, P., Propulsive performance of a continuously rotating detonation engine. *Journal of Propulsion and Power*, 27(1), 2011, pp.171-181.
19. Shen, D., Cheng, M., Wu, K., Sheng, Z., Wang, J., "Effects of supersonic nozzle guide vanes on the performance and flow structures of a rotating detonation combustor". *Acta Astronautica*, 193, 2022, pp.90-99.
20. Tsuboi, N., Eto, S., Hayashi, A. K., Kojima, T., "Front cellular structure and thrust performance on hydrogen–oxygen rotating detonation engine". *Journal of Propulsion and Power*, 33(1), 2017, pp.100-111.
21. Wang, Y., Wang, J., Qiao, W., "Effects of thermal wall conditions on rotating detonation". *Computers & Fluids*, 140, 2016, pp.59-71.
22. Salvadori, M., Tudisco, P., Ranjan, D., Menon, S., "Numerical investigation of mass flow rate effects on multiplicity of detonation waves within a H2/Air rotating detonation combustor". *International Journal of Hydrogen Energy*, 47(6), 2022, pp.4155-4170.
23. Sun, J., Zhou, J., Liu, S., Lin, Z., Lin, W., "Plume flowfield and propulsive performance analysis of a rotating detonation engine". *Aerospace Science and Technology,* 81, 2018, pp.383-393.
24. Zhang, C., Lin, Z., Dong, T., "Numerical study on the interaction characterization of rotating detonation wave and turbine rotor blades". *International Journal of Hydrogen Energy,* 47(10), 2022, pp.6898-6910.
25. Zhao, N., Meng, Q., Zheng, H., Li, Z., Deng, F., "Numerical study of the influence of annular width on the rotating detonation wave in a non-premixed combustor". *Aerospace Science and Technology*, 100, 2020, pp.105825.
26. Wiebe, R., Spottswood, S. M., "On the dimension of complex responses in nonlinear structural vibrations". *Journal of Sound and Vibration*, 373, 2016, pp. 192-204.
27. Schwer, D., Kailasanath, K., "Numerical study of the effects of engine size n rotating detonation engines". In *49th AIAA aerospace sciences meeting including the new horizons forum and aerospace exposition*, Orlando, USA: American Institute of Aeronautics and Astronautics, 2011, pp.581.
28. Zhong, Y., Wu, Y., Jin, D., Yang, X., Chen, X., "Rotating detonation mode recognition using non-intrusive vibration sensing". *Energy*, 199, 2020, pp.117466.